China Ocean Eng., 2020, Vol. 34, No. 1, P. 1–9
DOI: https://doi.org/10.1007/s13344-020-0001-0, ISSN 0890-5487
http://www.chinaoceanengin.cn/ E-mail: coe@nhri.cn

An Improved Method of Predicting Drag Anchor Trajectory Based on the Finite Element Analyses of Holding Capacity

QIAO Dong-sheng[a, *], GUAN Bo[a], LIANG Hai-zhi[a, b, *], NING De-zhi[a], LI Bin-bin[c], OU Jin-ping[a]

[a]State Key Laboratory of Coastal and Offshore Engineering, Dalian University of Technology, Dalian 116024, China

[b]School of Civil Engineering, Qingdao University of Technology, Qingdao 266520, China

[c]Sortec Offshore Pte. Ltd., 677670, Singapore

Received June 7, 2019; revised September 10, 2019; accepted October 14, 2019

Abstract

Drag anchor is one of the most commonly used anchorage foundation types. The prediction of embedded trajectory in the process of drag anchor installation is of great importance to the safety design of mooring system. In this paper, the ultimate anchor holding capacity in the seabed soil is calculated through the established finite element model, and then the embedded motion trajectory is predicted applying the incremental calculation method. Firstly, the drag anchor initial embedded depth and inclination angle are assumed, which are regarded as the start embedded point. Secondly, in each incremental step, the incremental displacement of drag anchor is added along the parallel direction of anchor plate, so the displacement increment of drag anchor in the horizontal and vertical directions can be calculated. Thirdly, the finite element model of anchor is established considering the seabed soil and anchor interaction, and the ultimate drag anchor holding capacity at new position can be obtained. Fourthly, the angle between inverse catenary mooring line and horizontal plane at the attachment point at this increment step can be calculated through the inverse catenary equation. Finally, the incremental step is ended until the angle of drag anchor and seabed soil is zero as the ultimate embedded state condition, thus, the whole embedded trajectory of drag anchor is obtained. Meanwhile, the influences of initial parameter changes on the embedded trajectory are considered. Based on the proposed method, the prediction of drag anchor trajectory and the holding capacity of mooring position system can be provided.

Key words: drag anchor, embedded trajectory prediction, increment calculation, holding capacity

Citation: Qiao, D. S., Guan, B., Liang, H. Z., Ning, D. Z., Li, B. B., Ou, J. P., 2020. An improved method of predicting drag anchor trajectory based on the finite element analyses of holding capacity. China Ocean Eng., 34(1): 1–9, doi: https://doi.org/10.1007/s13344-020-0001-0

1 Introduction

The offshore floating structures usually use mooring positioning system to positioning, of which anchorage system is a distinctly important part. The traditional drag anchor has many superiorities, such as low cost, mature technology, being able to be recycled and reused, and high ultimate holding capacity. Owing to the superiorities above, the traditional drag anchor is still diffusedly applied for mooring foundations. The anchor holding capacity is sensitive to the ultimate embedded depth, which is determined by the motion trajectory in the process of drag anchor installation. So, it is very useful to predict the embedded trajectory accurately.

The study of embedded trajectory of drag anchor usually considers two aspects: the ultimate embedded depth and the motion trajectory during the installation process. The drag anchor and mooring line during the installation process are shown in Fig. 1. The mooring line configuration can be divided into three parts: catenary, lying line, inverse catenary which is connected to the drag anchor directly. With the complexity and diversity of seabed soil, the type of mooring chain and the complex geometric structure of drag anchor can affect the motion mechanism of drag anchor, and

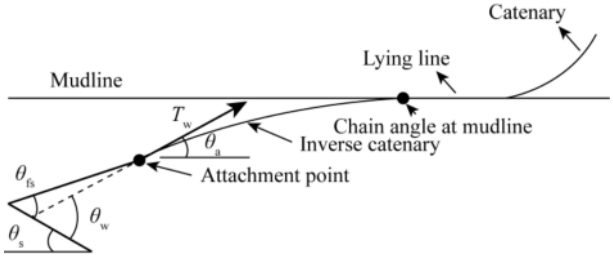

Fig. 1. Drag anchor and mooring line during the installation process.

Foundation item: This work was financially supported by the National Natural Science Foundation of China (Grant Nos. 51890915, 51490672, and 51761135011) and the Fundamental Research Funds for the Central Universities.

*Corresponding authors. E-mail: qiaods@dlut.edu.cn; mr_liangok@163.com

the drag anchor motion trajectory embedded into the seabed soil is extremely complex (Wu et al., 2016).

There are three main methods for the drag anchor motion trajectory prediction during the embedded process: model test, analytical and numerical simulation. The model test method, which includes field test, large scale test and small scale test, is typically considered as the most reliable (OMSI, 1990; Aubeny et al., 2008; Liu et al., 2010; O'Neill et al., 2003). The model test method can be used to measure the holding capacity, embedded trajectory, and drag anchor embedded depth by the scale of prototypical anchor (Degenkamp and Dutta, 1989; Neubecker and Randolph, 1996). Because of the scale effect, the small scale test cannot provide very accurate prediction results. Field test is mainly composed of JIPs (Joint Industry Projects) in the Gulf of Mexico to test some specific types of drag anchor, the cost is very expensive, and the test period is long. The geotechnical centrifuge is used to avoid the scale effect and simulate the actual geotechnical stress (Gaudin et al., 2010). The analytical method is usually used to simplify the inverse catenary and drag anchor, which uses the analytical expression to predict the drag anchor motion trajectory in the embedded process (Aubeny and Chi, 2010, 2014; Tian et al., 2015). Neubecker and Randolph (1995) obtained the inverse catenary state equation through the study of simplified stress analysis of the inverse catenary mechanics by transforming the mechanics equation into the state equation through small angle assumption. The inverse catenary equation concisely expresses the relation between tension and incline angle of the inverse catenary, and it is widely recognized and applied to the study of trajectory prediction by many scholars. The numerical simulation method is widely used in the ultimate drag anchor holding capacity calculation, which mainly uses the finite element simulation technology and considers the seabed soil and drag anchor interaction (Balasuriya, 2016; Zhao and Liu, 2016; Li et al., 2016).

The bottom of inverse catenary is connected to the drag anchor, so the embedded trajectory is the essential balance between inverse catenary and drag anchor at each embedded depth during the installation process (Ruinen and Degenkamp, 2002). At present, the inverse catenary effect is mainly calculated by the inverse catenary equation, while the anchor holding capacity is mainly calculated by the limit equilibrium method or upper bound plasticity method.

The limit equilibrium method is a typical incremental calculation process, which considerers the resistance forces of soil to anchor as the anchor holding capacity when the soil is under the failure condition. Ruinen (2004) proposed a method to predict the drag anchor motion trajectory in the embedded process on the base of the limit equilibrium theory, which is suitable for saturated soft clay by taking the attachment point as a reference point to establish the balance equations. Neubecker and Randolph (1996) used the inverse catenary state equation to describe the relationship between tensions and incline angle of inverse catenary, and applied the limit equilibrium method in the ultimate anchor holding capacity calculation at different positions, and then combined the incremental calculation method to predict the drag anchor motion trajectory in the embedded process.

The main difference between the upper bound plasticity method and limit equilibrium method is that the concept of plastic yield model on anchor plate is applied in the calculation of holding capacity of anchor plate and this method does not involve the stress analysis of anchor plate in the seabed soil. The plastic yield surface of seabed soil under multiple loads is calculated, and the virtual work principle is used to determine the anchor plate movement direction, then the drag anchor embedded trajectory can be predicted by incrementation. O'Neill et al. (2003) firstly introduced the plastic yield concept of drag anchor to the embedded trajectory prediction, and comprehensively considered the influence of anchor plate, anchor shank and inverse catenary on the trajectory. Aubeny and Chi (2010) used the yield function proposed by O'Neill et al. (2003), and combined it with the inverse catenary characteristics to predict the embedded trajectory method suitable for saturated soft clay.

The aim of this paper is to present an improved method for the drag anchor motion trajectory prediction in the embedded process based on N–R method (Neubecker and Randolph, 1996). The finite element model is established by utilizing the software ANSYS, and the interaction between soil and drag anchor is considered, so the ultimate drag anchor holding capacity at different locations could be calculated. The embedded trajectory is obtained through combining the ultimate holding capacity calculation by ANSYS and the incremental calculation.

2 Incremental calculation

In order to predict the drag anchor motion trajectory in the embedded process, the incremental calculation method is applied in this paper. The installation process of inverse catenary and drag anchor could be considered as the quasi-static problem because of the slow dragging speed. The drag anchor trajectory could be considered as the curves connected by a series of points when it is embedded in the seabed soil, in which each point could be obtained by an incremental calculation step. At each position, the inverse catenary mooring line tensile force T_a is equal to the ultimate drag anchor holding capacity T_w. During the initial installation, the drag anchor has certain velocity when it penetrates the seabed, so the initial embedded depth of anchor plate z_0 and the initial placement angle θ_{s0} are considered as known.

The stress analysis of inverse catenary is shown in Fig. 2, and the weight of anchor can be ignored based on Neubecker and Randolph's research (Neubecker and Randolph, 1996). The gravity of catenary is ignored and the angle of catenary at the seabed surface is assumed as zero,

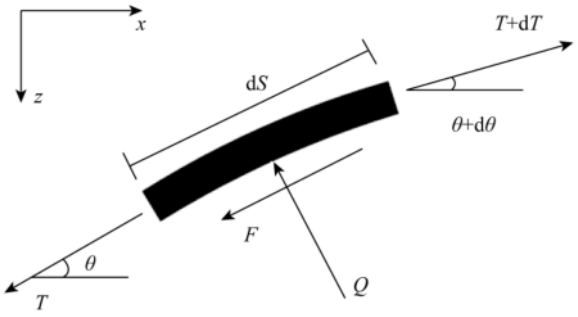

Fig. 2. Force analysis of mooring line element.

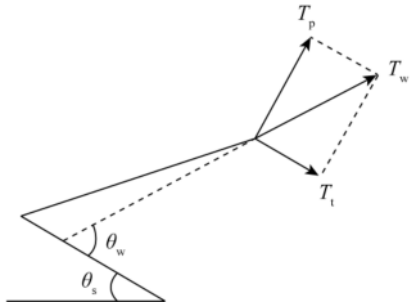

Fig. 3. Force equilibrium of drag anchor.

and then the equation of drag force T and angle θ can be obtained. The effect of inverse catenary mooring line acting on the anchor could be calculated in Eq. (1) at the attachment point:

$$T_a\theta_a^2/2 = D\overline{Q}, \tag{1}$$

where, T_a is the inverse catenary tensile force at the attachment point; θ_a is the angle between inverse catenary mooring line and horizontal plane at the attachment point; D is the drag anchor embedded depth; $\overline{Q}$ is the average resistance of seabed soil acting on the inverse catenary mooring line.

The average resistance $\overline{Q}$ can be calculated from Eq. (2):

$$\overline{Q} = N_c E_n d \int_0^z S_u \mathrm{d}z/D, \tag{2}$$

where, N_c is the non-dimensional holding capacity factor of inverse catenary for plane strain failure; E_n is the effective widths of inverse catenary in the normal direction; d is the inverse catenary nominal diameter; S_u is the seabed soil undrained shear strength; z is the drag anchor embedded depth.

During the embedding process, the drag anchor is assumed to move along the parallel direction of anchor plate at each incremental step, so the ultimate resistance force of soil to anchor can be considered as the ultimate drag anchor holding capacity. Neubecker and Randolph (1996) proposed the simplified analytical calculation as shown in Eq. (3). Alternatively, the ultimate drag anchor holding capacity is calculated by the finite element method in this paper.

$$T_p = fA_pN_c'S_u, \tag{3}$$

where, f is the drag anchor form factor; A_p is the anchor plate projected area; N_c' is the non-dimensional holding capacity factor of anchor.

By ignoring the self-weight of drag anchor, the tension from inverse catenary to drag anchor can be divided into T_p and T_t in the tangential and normal direction, respectively, as shown in Fig. 3 and Eq. (4). The angle between T_w and anchor plate, θ_w is dependent on the angle between anchor plate and shank, which can be assumed to be constant during the installation process (Neubecker and Randolph, 1996).

$$T_w = T_p/\cos\theta_w. \tag{4}$$

During the process of drag anchor being embedded into the seabed soil, the relationship between the angle θ_a and θ_s at any position can be calculated by Eq. (5) as shown in Fig. 1.

$$\theta_s = \theta_w - \theta_a. \tag{5}$$

Therefore, the incremental calculation of predicting drag anchor trajectory can be carried out according to the following steps, and the calculation flow diagram is shown in Fig. 4 (Qiao et al., 2018).

(1) The initial embedded depth of anchor plate z_0, the initial placement angle θ_{s0}, the parameters of seabed soil and anchor plate are input in the first incremental step.

(2) The displacement Δt is imposed along the parallel direction of anchor plate, by which the displacement of anchor plate along the horizontal direction Δx and the vertical embedded depth Δz can be obtained, so the new position of anchor can be obtained.

(3) The ultimate drag anchor holding capacity in the new position T_w can be calculated by Eqs. (3) and (4), or by the established finite element method in Section 3 of this paper.

(4) The inverse catenary angle θ_a at the new position can be calculated by Eq. (1), and here $T_w = T_a$.

(5) The angle between the horizontal plane and anchor plate θ_s at the new position can be calculated by Eq. (5).

(6) Continue Steps (1)−(5) until θ_s is 0, and then stop the incremental calculation to obtain the whole drag anchor embedded trajectory.

3 Finite element model of anchor

In the previous description above, the ultimate drag anchor holding capacity T_w should be re-calculated at every incremental step. The parameters which have influence on the ultimate drag anchor holding capacity, include the seabed soil, drag anchor embedded depth z and the angle between horizontal plane and anchor plate θ_s. Meanwhile, z and θ_s are varying at each incremental step, so the rebuilding of finite element models of anchor is necessary. In consideration of the accuracy and efficiency of finite element

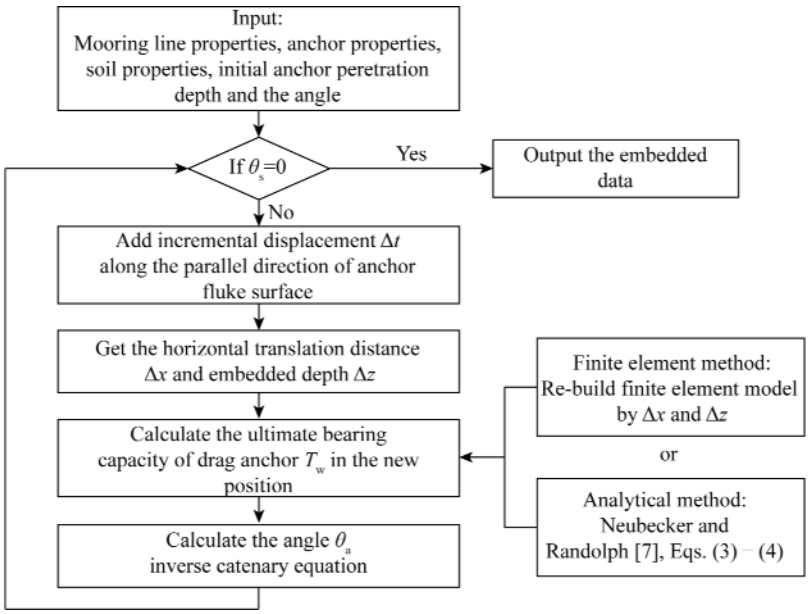

Fig. 4. Incremental calculation flow diagram.

calculation, the displacement increment in each incremental step Δt is chosen as 2 m in the numerical calculation.

The interaction between drag anchor and seabed soil is a frictional contact type. When defining the contact pairs, the seabed soil is selected as the contact element and the drag anchor is selected as the target element. The friction effect is described by using Coulomb Friction Model. In the established finite element model, the contact pairs are defined via Target 169 and Conta 172 finite elements, the seabed soil and anchor plate are simulated by Plane 182 finite element. After meshing and considering the effect of grid precision on the result, the model is finally divided into 4739 elements, of which four elements are drag anchor and 4735 elements are soil, as shown in Fig. 5. The displacement constraints are imposed on the left, right and lower sides of seabed soil, while the upper side is a free surface.

In each incremental step, an increasing displacement load along the direction of anchor shank is imposed, and then the curve of holding capacity of drag anchor-displacement load can be obtained.

4 Holding capacity

4.1 Constitutive model and geometric parameters

In this paper, the 15t Stevpris drag anchor is taken as the research object. During the established finite element calculation model, the simplified drag anchor model is established as shown in Fig. 6, which is in the same way as Neubecker and Randolph (1996). By ignoring the effect of shank, the length F_l, thickness F_h, and width F_w of the rectangular anchor plate are set as 3 m, 0.5 m, and 7 m, respectively.

In order to reduce the boundary effect, $10F_l$ is chosen as the width and length of seabed soil range in the established finite element model. The Poisson's ratio is 0.3, and the elastic module of drag anchor is 2.1×11^{10} Pa.

The saturated soft clay in the Gulf of Mexico (Sukumaran et al., 1999) is chosen as the research object of seabed soil. The ideal elastic-plastic model obeying Von-Mises yield criterion is applied to simulate the soil, so the yield stress should be $\sqrt{3}S_u$. The seabed soil undrained shear

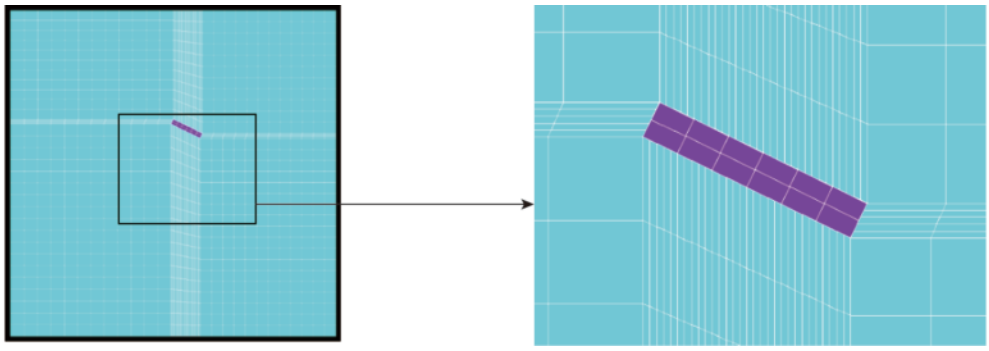

Fig. 5. Finite element model.

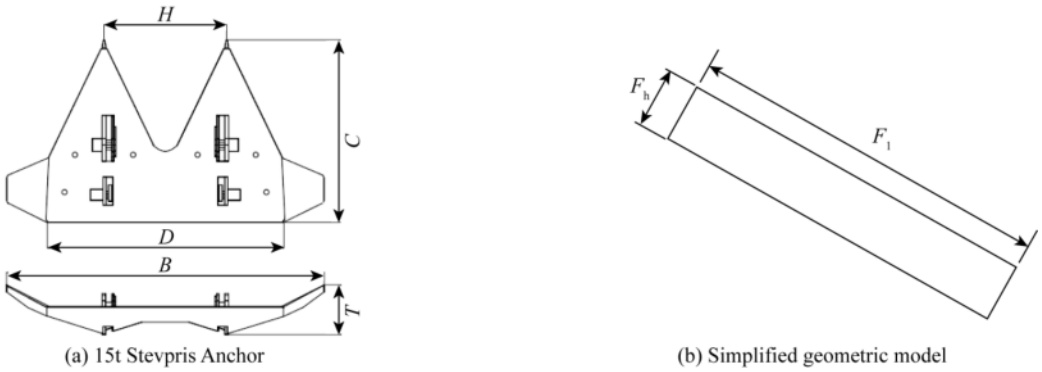

Fig. 6. Drag anchor model.

strength S_u is in proportion to depth H, which can be calculated by Eq. (6), and the seabed soil parameters are shown in Table 1.

$$S_u = S_0 + kH, \tag{6}$$

where, S_0 is the seabed soil undrained shear strength at the seabed surface; k is the increment of undrained shear strength per meter; H is the depth from seabed.

Table 1 Seabed soil constitutive and geometric parameters

Parameter name	Values
S_0 (kPa)	0
k (kPa/m)	1.26
E (Pa)	$1000S_u$
υ	0.49
Yield criterion	$\sqrt{3}S_u$

4.2 Finite element model validation

In order to validate the feasibility of calculating the drag anchor holding capacity using the established finite element model, the ultimate VLA Stevmanta holding capacity is calculated and the results are compared with the field test results of Ruinen (2004). The same parameters with the contrast results of model are adopted in the calculation as shown in Fig. 7.

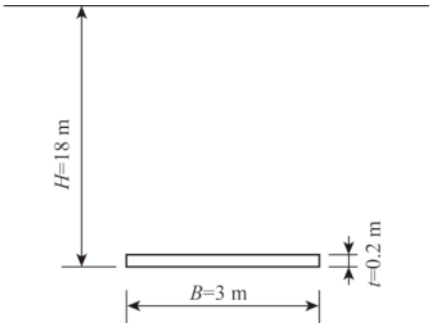

Fig. 7. Anchor plate calculation model (Ruinen, 2004).

The holding capacity-displacement load curve of drag anchor can be obtained according to the established finite element calculation method above, as shown in Fig. 8. The ultimate holding capacity calculation result obtained from the finite element model is 958.02 kN/m, while the result from Ruinen's field model test is 913.7 kN/m. The difference is 4.9%, which indicates that it is feasible to calculate the ultimate drag anchor holding capacity by using the established finite element model in this paper.

Furthermore, the ultimate drag anchor holding capacity is normalized and compared with the field test results of the Das (1978). The same model parameters are used in the calculation as shown in Fig. 9.

The normalized anchor holding capacity (N_c) obtained from the method above is shown in Fig. 10. It is further feasibly manifested that the established finite element model in this paper can be applied to the calculation of ultimate holding capacity.

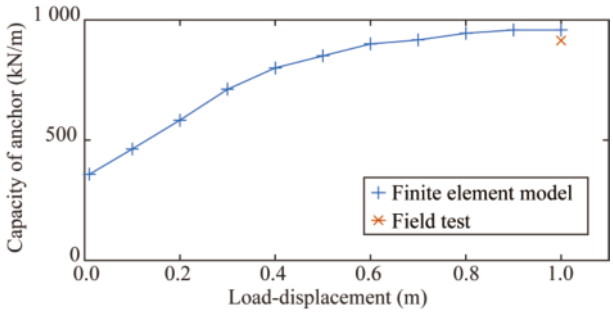

Fig. 8. Holding capacity-displacement load (model validation).

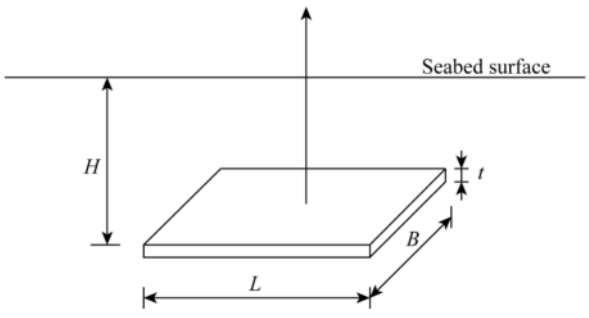

Fig. 9. Anchor plate calculation model (Sukumaran et al., 1999).

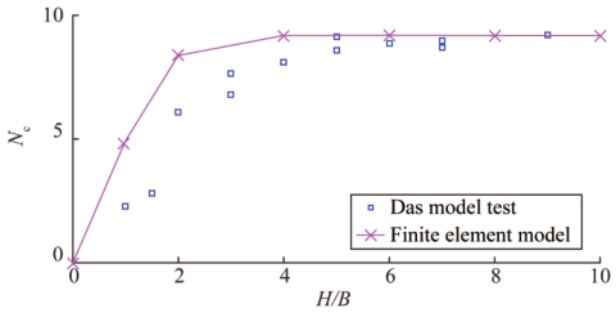

Fig. 10. Normalized holding capacity of anchor (model validation).

4.3 Holding capacity

With the established finite element model above, the holding capacity-displacement load curve at embedded depth of 10 m is shown in Fig. 11, and the corresponding normalized anchor holding capacity curve is shown in Fig. 12. The change trends under other embedded depths are the same. Figs. 13 and 14 show the maximum displacement and maximum plastic strain at different embedded depths, respectively.

According to Figs. 11 and 12, the holding capacity-displacement load curve could be divided into three obvious parts. Firstly, as the displacement load increases, the holding capacity increases linearly, which shows that the soil around drag anchor plate is at the elastic deformation stage without plastic deformation. Then, the holding capacity increases nonlinearly, which shows that plastic deformation occurs in the soil around drag anchor plate. Finally, with the displacement load continuing to increase, the holding capa-

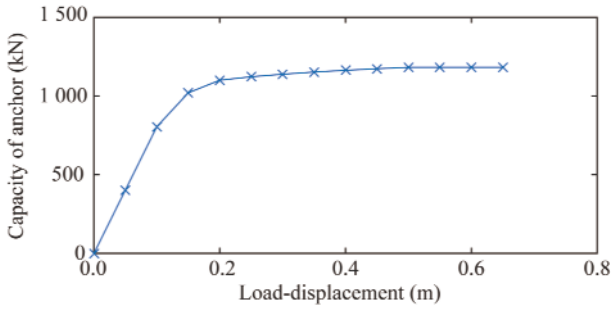

Fig. 11. Holding capacity-displacement load (depth H=10 m).

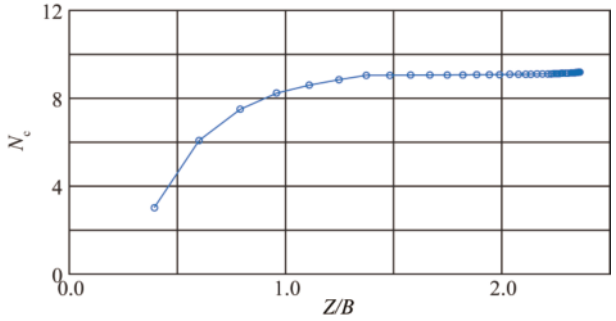

Fig. 12. Normalized anchor holding capacity.

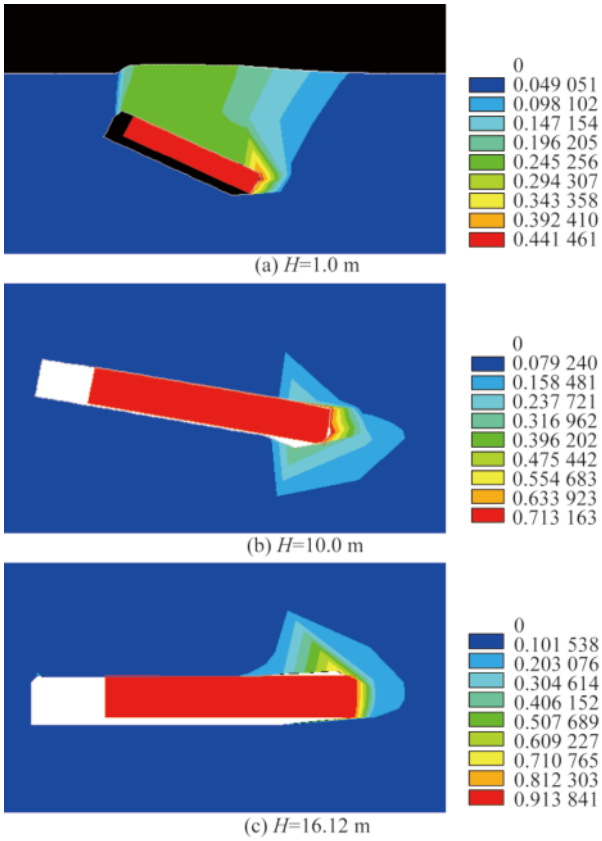

Fig. 13. Maximum displacement at different embedded depths.

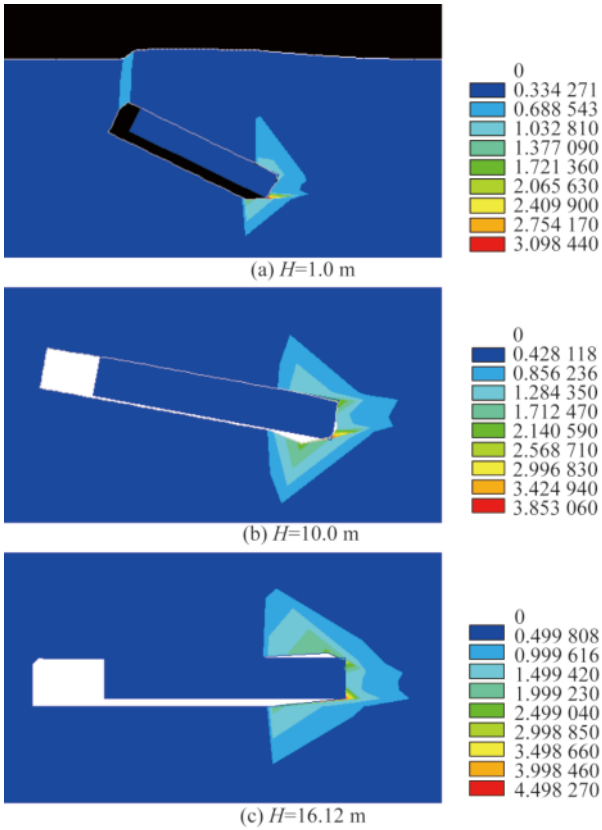

Fig. 14. Maximum plastic strain at different embedded depths.

city no longer increases and tends to a constant value, which shows that the soil around drag anchor plate reaches the ultimate condition, and this could be regarded as the ultimate drag anchor holding capacity at this embedded depth, that is T_w in Eq. (4).

According to Figs. 13 and 14, the failure modes of anchor plate are different at different embedded depths. The angles between horizontal plane and anchor plate at different embedded depths are different, which is determined by the trajectory prediction shown in Section 5. Under the condition of shallow embedded depth, the surrounded soil gradually spreads to the vertical direction of seabed surface, and then reaches the ultimate holding capacity. While under the condition of deep embedded depth, the surrounded soil gradually spreads to the direction parallel to the anchor plate, and then reaches the ultimate holding capacity. These different failure modes are the same as O'Neill (2003).

4.4 Influence of angle between horizontal plane and anchor plate

The influence of angle between horizontal plane and anchor plate θ_s on the ultimate holding capacity at the same embedded depth is studied. Three different embedded depths with three different θ_s are calculated, respectively, and the holding capacity-displacement curves are shown in Fig. 15.

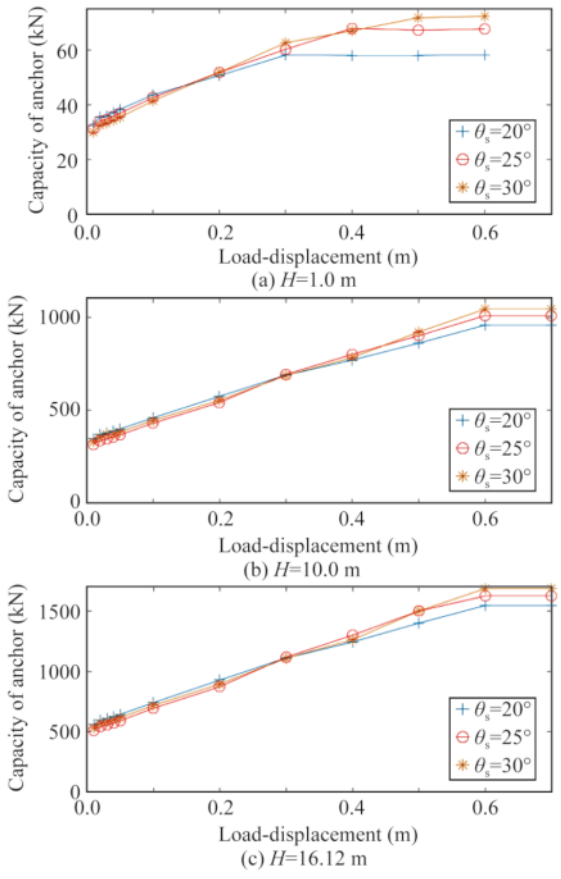

Fig. 15. Holding capacity-displacement load curves with different θ_s .

According to Fig. 15, the ultimate anchor holding capacity increases with the angle between horizontal plane and anchor plate θ_s increases at the same embedded depth. With the increase of embedded depth, the influence of θ_s on the ultimate holding capacity is getting smaller. The maximum difference of ultimate holding capacity with three angles at embedded depth of 1 m is 25%, and that both are 9% at embedded depths of 10 m and 16.12 m. The reason is that the failure module is different at shallow and deep embedded depths as shown above.

4.5 Influence of angle between the drag anchor tension and anchor plate

The influence of angle between drag anchor tension and anchor plate θ_w (the imposed direction of load) on the ultimate drag anchor holding capacity at the same position is studied. Three different θ_w at the embedded depth of 10 m are calculated, and the holding capacity-displacement load curves are shown in Fig. 16.

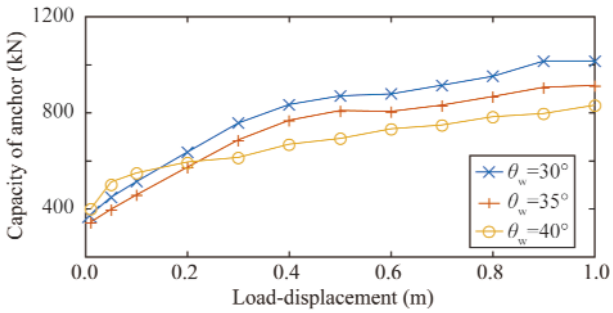

Fig. 16. Holding capacity-displacement load curves with different θ_w.

According to Fig. 16, the ultimate anchor holding capacity decreases with the angle between horizontal plane and anchor plate θ_w increasing at the same embedded depth. The maximum difference of ultimate holding capacity with three angles θ_w at embedded depth of 10 m is 22%, which indicates that angle θ_w has more influence than angle θ_s.

5 Trajectory prediction

5.1 Trajectory prediction method validation

As shown in Section 4, the 15t Stevpris drag anchor is taken as the study object in this paper, and then the incremental calculation method shown above is used to predict the anchor motion trajectory in the embedded process. Meanwhile, the trajectory prediction results obtained from Neubecker and Randolph (1996) who used the incremental calculation method based on analytical solution and Aubeny et al. (2008) who used the upper bound collapse load analysis method are also compared as shown in Fig. 17. The initial calculation parameters suggested by Neubecker and Randolph (1996) are: inverse catenary mooring line $E_n d$=0.16 m, embedded depth of anchor plate z_0=1 m, the

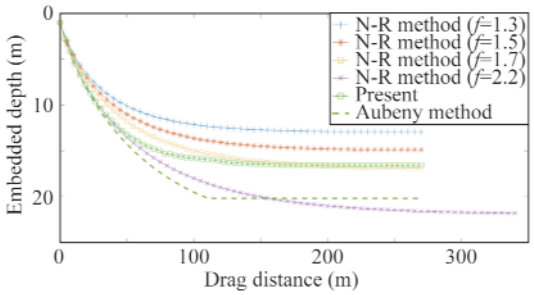

Fig. 17. Embedded trajectory of drag anchor.

angle between the anchor plate and horizontal plane θ_{s0}=25°, the angle between the drag anchor tension and anchor plate θ_w=35°, and form factor of drag anchor f=1.3. The other parameters are the same as in Section 4.1.

According to Fig. 17, the change law of embedded motion trajectory of anchor obtained from the presented method in this paper is in accordance with the results by the N−R method (Neubecker and Randolph, 1996) and Aubeny method (Aubeny et al., 2008). The change of embedded motion trajectory can be divided into three obvious parts: at the first part, the drag anchor motion is the directly translational penetration at the initial embedded angle; at the second part, the drag anchor motion is the rotary penetrating movement; at the final part, the drag anchor motion is the horizontal penetration. If the second part appears earlier, the final embedded depth will be smaller.

The core difference between the N−R method and the presented method in this paper is the drag anchor holding capacity calculation at different embedded depths at each incremental step. Eq. (3) is used in the N–R method, and it could be seen that the holding capacity factor N'_c is chosen as a constant value at different embedded depth. According to Fig. 12, the holding capacity factor N'_c changes clearly at different embedded depths, and the failure modes at different embedded depths are also different. So, using the present method in this paper should be more accurate with the actual situation of soil surround the anchor. Regarding as Aubeny's method (Aubeny et al., 2008), the upper bound collapse load analysis method is applied in the calculation of anchor holding capacity, where the plastic yield function is chosen.

The final embedded depth obtained from the presented method in this paper is 16.12 m, while that from the N–R method with suggested f=1.3 is 12.93 m. The different form factor f is chosen to predict the drag anchor embedded motion trajectory, and by contrast it can be found that the result by the presented method in this paper is closer to the results by the form factor f=1.7. These results indicate that the form factor of anchor has significant effects on the drag anchor embedded trajectory prediction, which is also concluded by O'Neill et al. (2003).

5.2 Influence of the angle between the horizontal plane and anchor plate

As the angle between the drag anchor tension and anchor plate is the same as the initial condition, which is set as θ_w=35°, the influence of angle between the horizontal plane and anchor plate θ_s on the embedded trajectory is studied. The trajectory prediction results with three different θ_s are shown in Fig. 18.

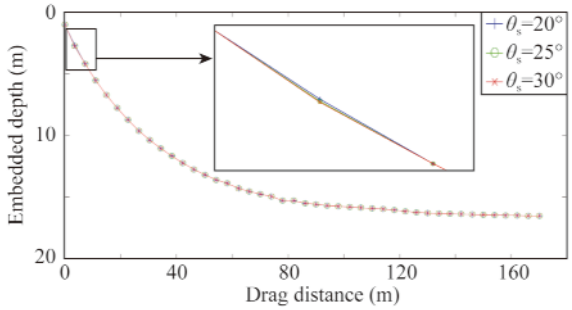

Fig. 18. Embedded trajectory with different θ_s.

According to Fig. 18, there are only slight differences among the three trajectories with different θ_s when the anchor is just embedded into the seabed. Combined with the holding capacity calculation results in Section 4.4, the specific calculation results at the first incremental step are shown in Table 2. After the first incremental calculation, the updated angle between the anchor plate and horizontal plane θ_s' is very close, and the corresponding drag distance and embedded depth are also very close. So, the following trajectories are very close, and it could be concluded that the initial angle between the horizontal plane and anchor plate θ_s has little influence on the trajectory prediction.

Table 2 Incremental calculation at the first step

θ_{s0}(°)	T_w (kN)	θ'_s(°)	Drag distance x (m)	Embedded depth z (m)
20°	72.32	25.92	0.89937	1.4372
25°	67.67	25.62	0.90170	1.4324
30°	58.17	24.88	0.90718	1.4207

5.3 Influence of the angle between the drag anchor tension and anchor plate

Since the angle between the horizontal plane and anchor plate is the same as the initial condition, which is set as θ_s=25°, the influence of angle between the drag anchor tension and anchor plate θ_w on the embedded trajectory is studied. The trajectory prediction results under three different θ_w are shown in Fig. 19.

According to Fig. 19, the change laws of three trajectories with different θ_w are similar, but the ultimate embedded depths are 12.78 m, 16.52 m, and 22.85 m, respectively. The ultimate embedded depth increases as the angle between the drag anchor tension and anchor plate θ_w increases. According to the calculation results of holding capacity in Section 4.5, the ultimate anchor holding capacity decreases as θ_w in-

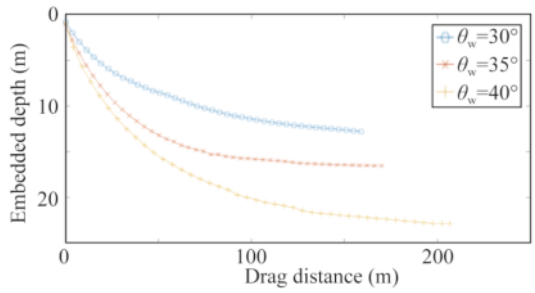

Fig. 19. Embedded trajectory under different θ_s.

creases, and the soil resistance of inverse catenary mooring line T_a could be considered the same with different θ_w. So, the ultimate embedded depth needs to be larger in order to resist T_a. It could be concluded that the angle between the drag anchor tension and anchor plate θ_w has significant influence on the trajectory prediction.

6 Conclusions

An improved method of predicting the drag anchor embedded trajectory combined with the incremental calculation method and finite element analyses of holding capacity is proposed in this paper. The 15t Stevpris anchor is taken as the study object, and the proposed method is validated and compared with N–R method. The influences of initial calculation parameters are also investigated. Some conclusions can be drawn from the results.

(1) With the increase of displacement, the anchor holding capacity increases, and the holding capacity-displacement curve can be divided into two three obvious parts: linearly increase with elastic deformation, nonlinearly increase with plastic deformation accumulation, no longer increase which could be regarded as the ultimate anchor holding capacity.

(2) The drag anchor plate failure modes are obviously different when the anchor is at large and small embedded depths.

(3) The drag anchor embedded motion trajectory can be also divided into three obvious parts: directly translational penetrating at the initial embedded angle, rotary penetrating movement, and horizontal penetration. The earlier the second part appears, the smaller the final embedded depth is obtained.

(4) The initial angle between the horizontal plane and anchor plate has little influence on the trajectory prediction, but the angle between the drag anchor tension and anchor plate has significant influence.

The proposed method in this paper which could be used to calculate the ultimate drag anchor holding capacity and to predict the embedded motion trajectory is feasible. In order to complete and improve this method, still some work is needed to be done, such as more comparisons with results of other published field tests and large experiment results, the weightless of anchor assumptions, and so on.

References

Aubeny, C. and Chi, C.M., 2010. Mechanics of drag embedment anchors in a soft seabed, *Journal of Geotechnical and Geoenvironmental Engineering*, 136(1), 57–68.

Aubeny, C. and Chi, C.M., 2014. Analytical model for vertically loaded anchor performance, *Journal of Geotechnical and Geoenvironmental Engineering*, 140(1), 14–24.

Aubeny, C.P., Murff, J.D. and Kim, B.M., 2008. Prediction of anchor trajectory during drag embedment in soft clay, *International Journal of Offshore and Polar Engineering*, 18(4), 314–319.

Balasuriya, S., 2016. A numerical scheme for computing stable and unstable manifolds in nonautonomous flows, *International Journal of Bifurcation and Chaos*, 26(14), 1630041.

Das, B.M., 1978. Model tests for uplift capacity of foundations in clay, *Soils and Foundations*, 18(2), 17–24.

Degenkamp, G. and Dutta, A., 1989. Soil resistances to embedded anchor chain in soft clay, *Journal of Geotechnical Engineering*, 115(10), 1420–1438.

Gaudin, C., Simkin, M., White, D.J. and O'Loughlin, C.D., 2010. Experimental investigation into the influence of a keying flap on the keying behaviour of plate anchors, *Proceedings of the 20th International Offshore and Polar Engineering Conference*, International Society of Offshore and Polar Engineers, Beijing, China.

Li, P.D., Liu, H.X. and Zhao, Y.B., 2016. Large deformation finite element analysis on the kinematic behavior of drag anchors in the seabed, *The Ocean Engineering*, 34(2), 56–63. (in Chinese)

Liu, H.X., Zhang, W. and Zhang, X.M., 2010. Experimental investigation on the penetration mechanism and kinematic behavior of drag anchors, *Applied Ocean Research*, 32(4), 434–442.

Neubecker, S.R. and Randolph, M.F., 1995. Profile and frictional capacity of embedded anchor chains, *Journal of Geotechnical Engineering*, 121(11), 797–803.

Neubecker, S.R. and Randolph, M.F., 1996. The performance of drag anchor and chain systems in cohesive soil, *Marine Georesources and Geotechnology*, 14(2), 77–96.

Omega Marine Services International, 1990. Joint industry project: Gulf of mexico large scale anchor tests—test report, Houston: Omega Marine Services International.

O'Neill, M., Bransby, M.F. and Randolph, M.F., 2003. Drag anchor fluke-soil interaction in clays, *Canadian Geotechnical Journal*, 40(1), 78–94.

Qiao, D.S., Bao, M., Yan, J., Zhou, D.C. and Li, Y.G., 2018. A method to predict embedded trajectory based on the finite element analyses of bearing capacity of drag anchor, *Proceedings of the ASME 37th International Conference on Ocean, Offshore and Arctic Engineering*, ASME, Madrid, Spain.

Ruinen, R. and Degenkamp, G., 2002. Prediction of the holding capacity and trajectory of drag embedment anchors, *Proceedings of the Offshore Technology Conference*, OTC, Houston, Texas, pp. 52−54.

Ruinen, R.M., 2004. Penetration analysis of drag embedment anchors in soft clays, *Proceedings of the 14th International Offshore and Polar Engineering Conference*, International Society of Offshore and Polar Engineers, Toulon, France.

Sukumaran, B., McCarron, W.O., Jeanjean, P. and Abouseeda, H., 1999. Efficient finite element techniques for limit analysis of suction caissons under lateral loads, *Computers and Geotechnics*, 24(2), 89–107.

Tian, Y., Randolph, M.F. and Cassidy, M.J., 2015. Analytical solution for ultimate embedment depth and potential holding capacity of plate anchors, *Géotechnique*, 65(6), 517–530.

Wu, X., Chow, Y.K. and Leung, C.F., 2016. Prediction of drag anchor trajectory with both shallow and deep anchor behavior, *Proceedings of the Offshore Technology Conference Asia*, OTC, Kuala Lumpur, Malaysia.

Zhao, Y.B. and Liu, H.X., 2016. Numerical implementation of the installation/mooring line and application to analyzing comprehensive anchor behaviors, *Applied Ocean Research*, 54, 101–114.